🔓 OPEN ACCESS

Conjugated polymers based on metalla-aromatic building blocks

Shiyan Chen[a,b] 🔟, Lixia Peng[a] 🔟, Yanan Liu[a], Xiang Gao[a], Ying Zhang[a], Chun Tang[b], Zhenghao Zhai[a], Liulin Yang[a] 🔟, Weitai Wu[a], Xumin He[a], Liu Leo Liu[b] 🔟, Feng He[b], and Haiping Xia[a,b,1] 🔟

Conjugated polymers usually require strategies to expand the range of wavelengths absorbed and increase solubility. Developing effective strategies to enhance both properties remains challenging. Herein, we report syntheses of conjugated polymers based on a family of metalla-aromatic building blocks via a polymerization method involving consecutive carbyne shuttling processes. The involvement of metal d orbitals in aromatic systems efficiently reduces band gaps and enriches the electron transition pathways of the chromogenic repeat unit. These enable metalla-aromatic conjugated polymers to exhibit broad and strong ultraviolet–visible (UV–Vis) absorption bands. Bulky ligands on the metal suppress π–π stacking of polymer chains and thus increase solubility. These conjugated polymers show robust stability toward light, heat, water, and air. Kinetic studies using NMR experiments and UV–Vis spectroscopy, coupled with the isolation of well-defined model oligomers, revealed the polymerization mechanism.

conjugated polymers | metallopolymers | metalla-aromatics | stepwise polymerization

Conjugated polymers are macromolecules usually featuring a backbone chain with alternating double and single bonds (1–3). These characteristics allow the overlapping p-orbitals to form a system with highly delocalized π-electrons, thereby giving rise to intriguing chemical and physical properties (4–6). They have exhibited many applications in organic light-emitting diodes, organic thin film transistors, organic photovoltaic cells, chemical sensors, bioimaging and therapies, photocatalysis, and other technologies (7–10). To facilitate the use of solar energy, tremendous efforts have been devoted in recent decades to developing previously unidentified conjugated polymers exhibiting broad and strong absorption bands (11–13). The common strategies for increasing absorption involve extending π-conjugation by incorporating conjugated cyclic moieties, especially fused rings; modulating the strength of intramolecular charge transfer between donor and acceptor units (D–A effect); increasing the coplanarity of π conjugation through weak intramolecular interactions (e.g., hydrogen bonds); and introducing heteroatoms or heavy atoms into the repeat units of conjugated polymers (11–16). Additionally, appropriate solubility is a prerequisite for processing and using polymers and is usually achieved with the aid of long alkyl or alkoxy side chains (12, 17).

Aromatic rings are among the most important building blocks for conjugated polymers. In addition to aromatic hydrocarbons, a variety of aromatic heterocycles composed of main-group elements have been used as fundamental components. These heteroatom-containing conjugated polymers show unique optical and electronic properties (4–10). However, while metalla-aromatic systems bearing a transition metal have been known since 1979 due to the pioneering work by Thorn and Hoffmann (18), none of them have been used as building blocks for conjugated polymers. The HOMO–LUMO gaps (E_g) of metalla-aromatics are generally narrower (Fig. 1) than those of their organic counterparts (19–22). We reasoned that this feature should broaden the absorption window if polymers stemming from metalla-aromatics are achievable.

In recent years, we have reported a series of readily accessible metal-bridged bicyclic/polycyclic aromatics, namely carbolong complexes, which are stable in air and moisture (23–25). The addition of osmium carbynes (in carbolong complexes) and alkynes gave rise to an intriguing family of d_π–p_π conjugated systems, which function as excellent electron transport layer materials in organic solar cells (26, 27). These observations raised the following question: Can this efficient addition reaction be used to access metalla-aromatic conjugated polymers? It is noteworthy that incorporation of metalla-aromatic units into conjugated polymers is hitherto unknown. In this contribution, we disclose a polymerization reaction involving M≡C analogs of C≡C bonds, which involves a unique carbyne shuttling strategy (Fig. 2A). This led to examples of metalla-aromatic conjugated polymers (polycarbolongs) featuring metal carbyne units in the main chain. On the other hand, the development of polymerization reactions plays a crucial role in involving certain building blocks in conjugated polymers (28–32). These

Significance

Conjugated polymers have attracted great attention because of their promising physical properties. Aromatic moieties are often fundamental building blocks of conjugated polymer skeletons. Inclusion of transition metals, with their d orbitals, into aromatic frameworks results in d_π–p_π conjugated metalla-aromatic systems, which have interesting physical properties. However, such metalla-aromatics have never been used as building blocks in the backbones of conjugated polymers. Herein, we report a polymerization reaction of alkynes and carbynes that affords metalla-aromatic conjugated polymers. This efficient stepwise polymerization involves consecutive carbyne shuttling processes. These metallopolymers not only are soluble and stable but also exhibit broad and strong ultraviolet absorption. It is anticipated that these d_π–p_π conjugated polymer systems will find applications in materials science.

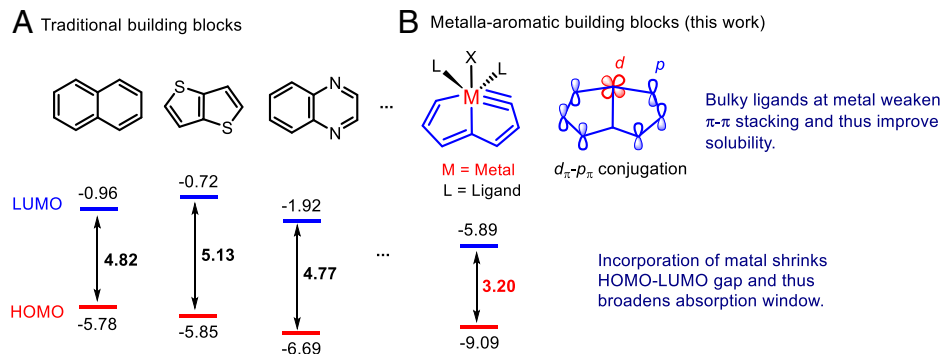[1]To whom correspondence may be addressed. Email: xiahp@sustech.edu.cn.

Fig. 1. Comparison of traditional organic skeletons with metalla-aromatic building blocks (the computed energies are in eV). (*A*) HOMO–LUMO gaps of classic aromatic skeletons. (*B*) Carbolong frameworks as potential building blocks for novel conjugated polymers with broad absorption bands and improved solubility.

efficient, specific, and feasible polymerizations could open an avenue for the synthesis of conjugated polymers.

Results and Discussion

As shown in Fig. 1, computational investigations revealed that the HOMO–LUMO gap (E_g) of the simplified model carbolong complex is 3.20 eV, which is lower than those calculated for pure organic aromatic skeletons such as naphthalene ($E_g = 4.82$ eV), thieno[3,2-b]thiophene ($E_g = 5.13$ eV), and quinoxaline ($E_g = 4.77$ eV). We thus envisioned that the small E_g should make such metalla-aromatic frameworks promising building blocks for conjugated polymers with unique properties.

In targeting metalla-aromatic conjugated polymers, a series of monomers (**1–5**) featuring a metallabicycle and a terminal alkyne with diverse spacer groups were synthesized via the reactions of multiyne carbon chains (**L1–L5**) with commercially available OsCl$_2$(PPh$_3$)$_3$ and PPh$_3$ (Fig. 2*B*). These monomers were characterized by NMR spectroscopy, elemental analysis (EA), and

high-resolution mass spectrometry (HRMS) (*SI Appendix*, Figs. S1–S87). The connectivity of **1b**, **2b**, and **3** was also unambiguously confirmed by X-ray diffraction (Fig. 2*B* and *SI Appendix*, Figs. S88–S90).

With **1–5** in hand, attempts to polymerize such monomers were undertaken. Treatment of **1–5** with HCl·Et$_2$O (0.20 M) in dichloromethane (DCM) at room temperature (RT) under a N$_2$ atmosphere for 24 h afforded polycarbolongs **P1–P5** (Table 1). Indeed, the formation of polymers containing **1a** and **3** was complete in 30 min, illustrating the high efficiency of the polymerization reaction. In view of the various reactivities of different monomers, we allowed the polymerizations to proceed for 24 h to ensure complete conversion. Addition of ether to the crude mixtures led to rapid precipitation of **P1–P5**, which were isolated in high yields after multiple washes with tetrahydrofuran. Multinuclear NMR spectra of **P1–P5** provided the structures of the polycarbolongs (*SI Appendix*, Figs. S91–S118). In the ^{31}P NMR spectra, these polycarbolongs displayed resonances at ~4.5 and −1.0 ppm, which are attributable to CPPh$_3$
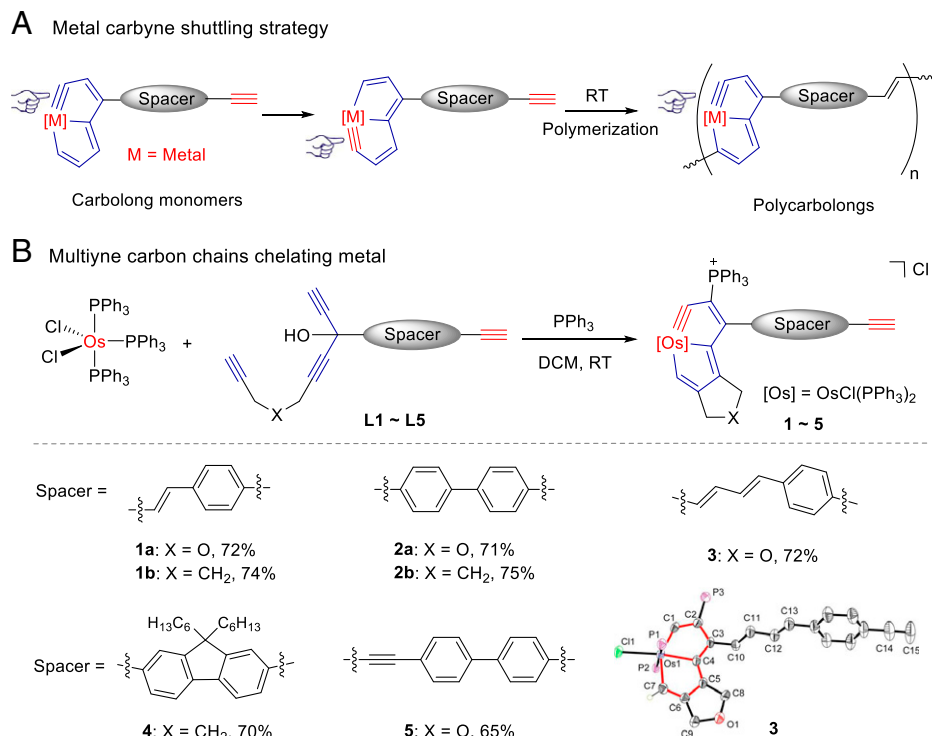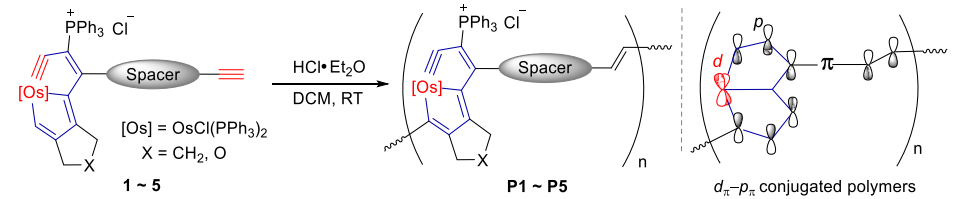

Fig. 2. Design of polymers and synthesis of monomers. (*A*) Schematic illustration of the polymerization strategy. (*B*) Preparation of carbolong monomers. Insert: X-ray molecular structure for the cations of complex **3**. Ellipsoids are shown at the 50% probability level; phenyl groups in PPh$_3$ are omitted for clarity.

Table 1. General applicability of the polymerization process.

Spacer	X group	Polymer	Yield*	M_n/M_w (kDa)[†]	$Đ$[†]
(styryl-phenyl spacer)	O	**P1a**	99%	30.5/41.5	1.35
	CH₂	**P1b**	98%	33.5/37.7	1.12
(biphenyl spacer)	O	**P2a**	97%	37.4/47.0	1.26
	CH₂	**P2b**	97%	37.9/47.5	1.25
(butadienyl-phenyl spacer)	O	**P3**	98%	40.5/59.7	1.47
(dihexylfluorene spacer)	CH₂	**P4**	95%	48.1/72.6	1.51
(ethynyl-biphenyl spacer)	O	**P5**	97%	39.7/57.5	1.45

*Polymerization conditions: monomers (20 mM) and HCl·Et₂O (0.20 M) in DCM under a N₂ atmosphere at RT for 24 h. Yields are for isolated products.

[†]Determined by gel permeation chromatography in DMF with 4.0 g/L LiBr salt added on the basis of a linear polystyrene calibration. Number-average molecular weight (M_n). Weight-average molecular weights (M_w). $Đ = M_w/M_n$.

and OsPPh₃, respectively (*SI Appendix,* Fig. S119). Gel permeation chromatographic studies indicated good average molecular weights and low polydispersities ($Đ$). Notably, **P1–P5** are highly stable and can be stored in air at RT for more than 2 y without noticeable decomposition. In all cases, thermolysis at

373 K for 2 h in air or exposure to white light for 96 h showed the apparent inertness (*SI Appendix,* Figs. S120 and S121).

The ultraviolet–visible (UV–Vis) spectroscopic features of polycarbolongs are summarized in Fig. 3*A*. The characteristic energy absorption bands showed λ_{max} values that varied between spacer
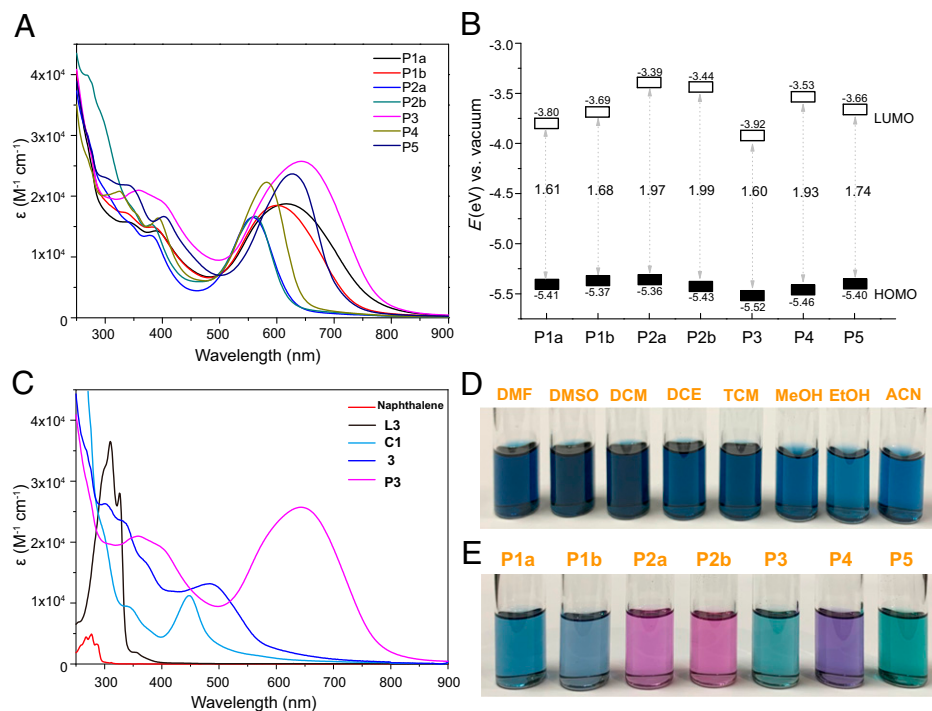

Fig. 3. Physical properties and solubility. (*A*) UV–Vis absorption spectra of polycarbolongs (1.0 × 10⁻⁵ M) measured in DCM at RT. Molar absorption coefficients were calculated based on repeat units. (*B*) HOMO and LUMO energies and energy gaps of polycarbolongs. (*C*) UV–Vis absorption spectra of naphthalene, multiyne carbon chains **L3**, simple carbolong framework **C1**, monomer **3**, and polycarbolong **P3** measured in DCM at RT (1.0 × 10⁻⁵ M). (*D*) Polycarbolong **P1a** dissolved in eight different solvents (1.0 × 10⁻⁴ M), 1,2-dichloroethane (DCE), trichloromethane (TCM), acetonitrile (ACN). (*E*) Different polycarbolongs dissolved in DCM (1.0 × 10⁻⁵ M).
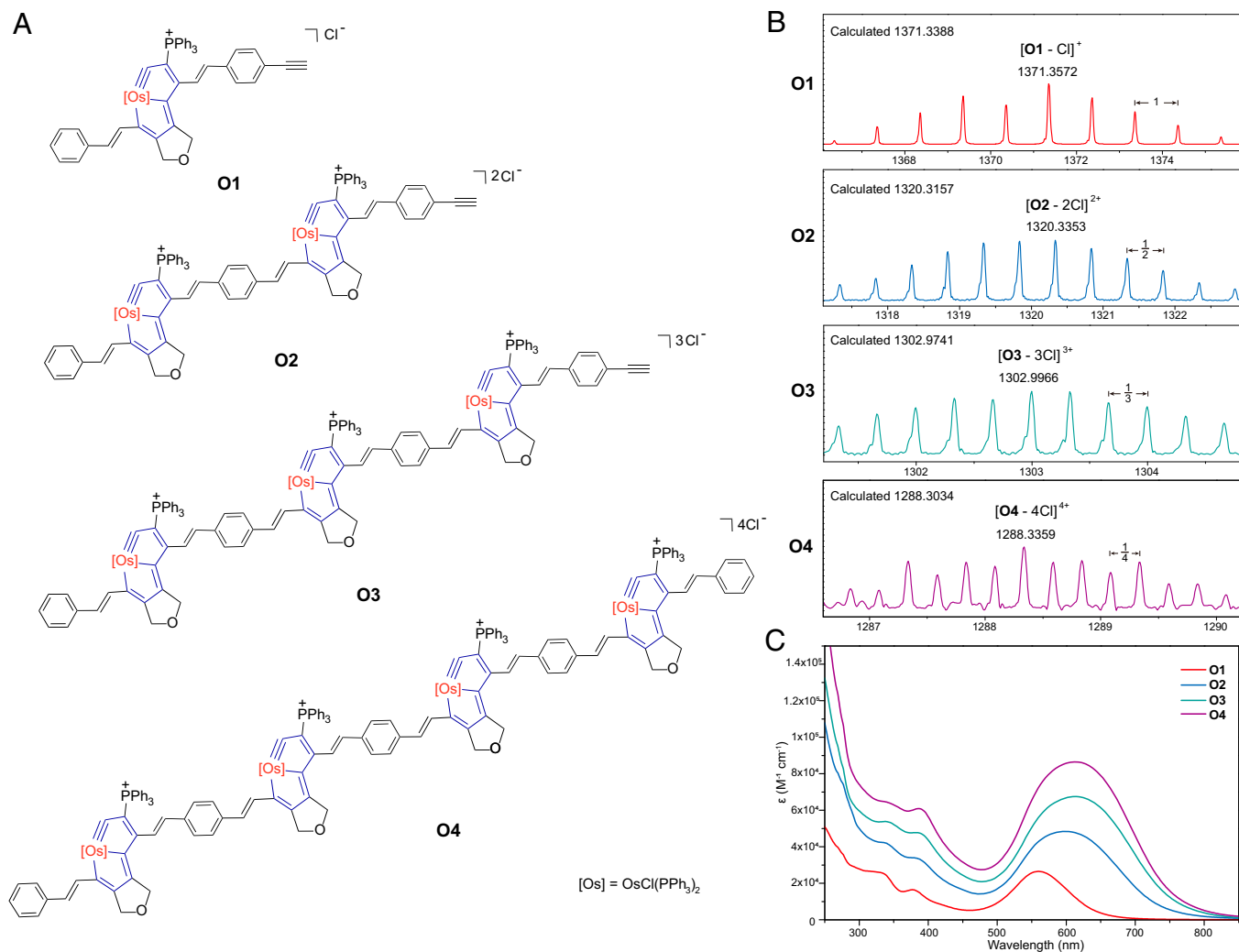
Fig. 4. Syntheses of oligomers. (*A*) Molecular structures of oligomers. (*B*) HRMS spectra of oligomers **O1–O4**. (*C*) UV–Vis absorption spectra of oligomers **O1–O4** (1.0 × 10⁻⁵ M) measured in DCM at RT.

groups (ranging from 550 to 650 nm). These λ_{max} values were more redshifted than those of other skeletal conjugated metallo-polymers, including polymetallaynes, polymetallocenes, and poly-metallocyclopentadiene (33–36). In particular, polycarbolong **P3** exhibited a broad and strong absorption band covering the entire UV–Vis region, even extending to the near-infrared (NIR) region. Its molar absorption coefficient at 650 nm was as high as 2.6 × 10⁴/M/cm. Polycarbolongs **P1–P5** are composed of metalla-aromatic repeating units and simple spacers, including styryl, biphenyl, butadiene-phenyl, fluorenyl, and ethynylbiphenyl. It is important to note that pure organic conjugated polymers based on these spacers do not exhibit such broad and strong absorption features (37–40). Polycarbolong **P4** can be regarded as an alternative copolymer of a metalla-aromatic and fluorenylene vinylene. While the absorption edge of poly(fluorenylene vinylene) reached only 460 nm (39), that of **P4** was remarkably redshifted up to 680 nm.

In addition, the molar absorption coefficient of **P4** was considerably larger (2.2 × 10⁴/M/cm; λ_{max} = 585 nm) than that observed for poly(fluorenylene vinylene) (9.9 × 10³/M/cm; λ_{max} = 400 nm) (39). The strong absorptions of **P1–P5** in the low-energy region resulted in a broad absorption window extending from UV to visible wavelengths and even into the NIR region. The characteristic energy absorption bands of polycarbolongs observed in films were similar to those in dilute

solutions (*SI Appendix*, Fig. S123). Collectively, these results indicate that the introduction of such metalla-aromatic frameworks into conjugated polymeric structures significantly affected the electronic properties.

To get more insight into the absorption contribution of polycarbolongs, the UV–Vis absorption of ligands (**L1–L5**) and monomers (**1–5**) was investigated (*SI Appendix*, Fig. S124 and S125). As shown in Fig. 3*C*, the characteristic absorption band of simple carbolong framework **C1** (*SI Appendix*, Fig. S126 for detail structure) is redshifted and enhanced compared to that of naphthalene. The characteristic absorption band of monomer **3** is also redshifted compared to that of its precursor ligand **L3**. These results indicate that the inclusion of the heavy atom osmium into an aromatic framework results in effects on the absorption property. With connecting spacer group, the λ_{max} of **3** (484 nm) is redshifted compared to that of **C1** (447 nm). It is noteworthy that no absorption peak in the low-energy region is detected in **L3**, **C1**, or **3**. It reveals that the repeat spacer and carbolong units make little contribution to the absorption of polycarbolongs. In comparison with the absorption spectra of **C1**, **3**, and **P3**, the characteristic absorption band is redshifted and enhanced with the extended π-conjugation. Hence, the high degree of delocalization in polycarbolongs is the main reason for their excellent absorption properties. Indeed, the actual redshifts observed between carbolong units and polycarbolongs
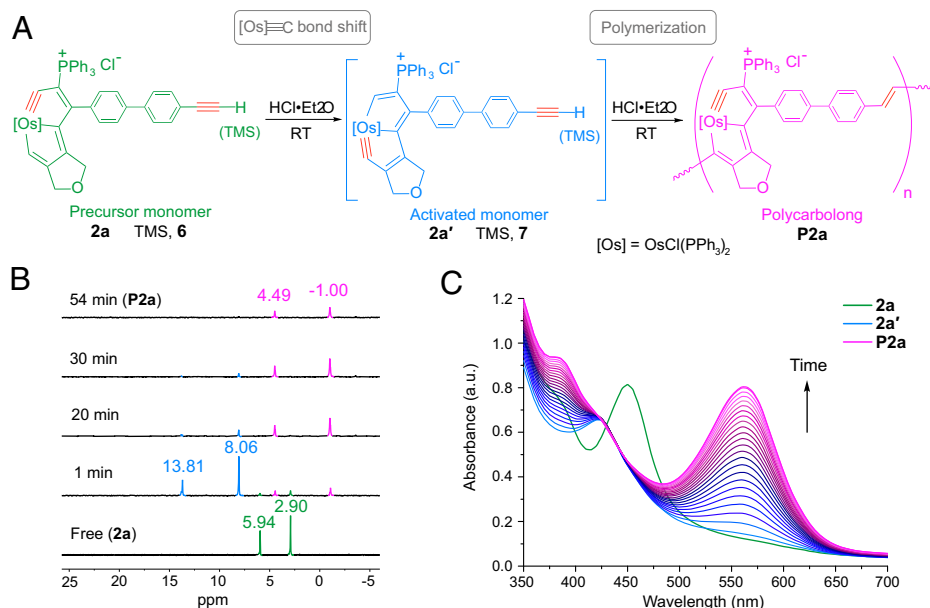
Fig. 5. Monitoring the polymerization reactions. (*A*) Metal carbyne shuttling strategy. (*B*) Stacked ^{31}P NMR spectra showing the conversion of precursor monomer **2a** into activated monomer **2a'** and polycarbolong **P2a**. (*C*) Generation of polycarbolong **P2a** in DCM at RT monitored in situ by UV–Vis spectroscopy (initial concentration 1.0×10^{-3} M).

are comparable to those for common conjugated polymers such as polythiophenes, poly(phenylenevinylene), and analogs (4–8).

To understand the cumulative effects of metalla-aromatics, the corresponding oligomers **O1–O4** (Fig. 4*A*) were synthesized and characterized (Fig. 4*B* and *SI Appendix*, Figs. S127–S142). With increases in the number of repeating units, the systems of delocalized π-electrons were more extended, and E_g decreased. Using density functional theory (DFT) calculations, the E_g values of oligomers **O1**, **O2**, and **O3** were calculated as 2.39, 2.02, and 1.77 eV, respectively. These oligomers exhibited strong π-electron delocalization, which was reflected by the calculated distribution of frontier molecular orbitals (*SI Appendix*, Fig. S143). As a result, the characteristic lowest-energy absorption bands of oligomers were significantly redshifted and enhanced as the oligomer size was increased (Fig. 4*C*).

The energy gaps of **P1–P5** were probed. The UV–Vis results combined with electrochemical analyses (*SI Appendix*, Fig. S174) revealed that the LUMO energies of **P1–P5** ranged from –3.92 eV (**P3**) to –3.39 eV (**P2a**), while E_g ranged from 1.60 eV (**P3**) to 1.99 eV (**P2b**) (Fig. 3*B*). For comparison, traditional conjugated polymers usually require comprehensive strategies (e.g., enough fused rings or a strong D–A effect) to achieve such a narrow E_g (11–13). These results suggest that altering the spacer group largely modulated the energy gaps of **P1–P5,** and such polycarbolongs with such diverse energy levels should have potential for many applications.

Note that many conjugated polymers with strong π–π stacking of their molecular chains are poorly soluble. A general strategy for increasing the solubility of these polymers involves decoration with long alkyl or alkoxy side chains (12, 17). Nonetheless, even without the aid of long carbon chains, the solubilities of **P1–P3** and **P5** in common organic solvents were good. As shown in Fig. 3*D*, polycarbolong **P1a** was soluble in diverse solvents (*SI Appendix*, Fig. S144 for a detailed solubility experiment). The maximum solubility in dimethyl sulfoxide (DMSO) and *N,N*-dimethylformamide (DMF) can reach 33.6 and 27.2 mg/mL, respectively. Interestingly, polycarbolongs **P1–P5** exhibited different colors in DCM (Fig. 3*E*). The greater solubility of **P1–P5** can be attributed to the osmium centers bearing sterically encumbering

ligands in the axial position, which precluded π–π stacking of polymer chains. The large PPh$_3$ substituent that helps to sterically protect the spacer group and the polycationic nature of the polymer probably also affect the observed polymer solubility. This method provided a way to modulate the solubility of conjugated polymers via installation of bulky transition metal fragments.

We next investigated polymerization of monomer **2a** (Fig. 5 and *SI Appendix*, Figs. S145 and S146). Upon treating **2a** with HCl·Et$_2$O, ^{31}P NMR spectroscopic monitoring revealed rapid consumption of **2a** (5.94 and 2.90 ppm [in green]) and immediate formation of **2a'** (13.81 and 8.06 ppm [in blue]) and **P2a** (4.49 and –1.00 ppm [in pink]). Species **2a'** was formed via a carbyne shift process and can be considered an activated monomer, and it was completely converted to **P2a** within ~1 h. To further confirm the structure of **2a'**, analogous compound **6**, in which the H atom in the terminal alkyne of **2a** was replaced with trimethylsilyl (TMS), was prepared. Compound **6** reacted with HCl·Et$_2$O to give isolable carbyne shift product **7**. The ^{31}P NMR resonances of **7** (13.71 and 8.07 ppm) and **2a'** were comparable (*SI Appendix*, Figs. S147–S159). To reveal the polymerization process, Fourier transform infrared spectrometry was used to monitor the formation of polycarbolong **P2a** (*SI Appendix*, Fig. S160). The C≡C–H and C≡C stretching vibrations of **2a** at 3,211/cm and 2,078/cm, respectively, disappeared gradually. Meanwhile, the C=C stretching vibration at 1,620/cm became stronger. This indicates that the C≡C bonds were efficiently converted to C=C bonds. The corresponding mechanisms for the polymerization reactions are shown in *SI Appendix*, Fig. S162. In view of the efficiency, specificity, and feasibility of this newly discovered stepwise polymerization between metal–carbon triple bonds and carbon–carbon triple bonds, we suggest that it could be designated as "metal-involved triple bond polymerization (MTP)."

These data are suggestive of an intriguing carbyne shuttling mechanism for the polymerizations. In **1–5**, the metal carbyne (i.e., Os≡C) was stabilized by protection from the proximal bulky triphenylphosphonium substituents. Accordingly, such monomers are bench stable and were readily purified by column chromatography in air. This ensured the preparation of high-quality

polycarbolongs. Nevertheless, under acidic conditions, **1–5** were readily transformed to Os≡C bond-shifted intermediates **1′–5′** via a carbyne shuttling reaction. Species **1′–5′** feature a less sterically protected Os≡C bond, which allowed effective polymerization reactions with terminal alkynes to form **P1–P5**, the first conjugated polymers with metal carbyne units in the main chain. After polyaddition, the carbyne reverted to the initial dormant state and was protected by the bulky triphenylphosphonium substituents, which stabilized the polycarbolongs toward light, heat, water, and air.

To gain insights into the kinetics of the polymerization, UV–Vis spectroscopy was used, and the formation of **P2a** from **2a** was monitored. As shown in Fig. 5*C*, **2a** (λ_{max} = 450 nm, in green) was completely consumed upon addition of HCl·Et₂O, which generated **2a′** (λ_{max} = 420 nm, in blue). No intermediate was observed. The characteristic UV absorption bands were consistent with those of model complexes **6** and **7** (*SI Appendix,* Fig. S163). Following this, a new absorption peak at 565 nm (in purple) derived from **P2a** appeared and gradually increased in intensity. In comparison with the band locations in the absorption spectra of **2a** and **P2a**, the characteristic energy absorption band was red-shifted from 450 nm to 565 nm, revealing that π-conjugation was extended during polymerization. The time-dependent peak intensity for the peak at 565 nm and kinetic variations in the in situ UV–Vis absorption spectra were recorded to follow the generation of **P2a** (*SI Appendix,* Fig. S164). These results showed that the polymerization was efficient. Besides, the formation of both **P1a** and **P3** was monitored by NMR and UV–Vis spectroscopic studies (*SI Appendix,* Fig. S165–S172). Similar consecutive carbyne shuttling processes can be observed during this polymerization.

Conclusions

We have shown examples of conjugated polymers based on metalla-aromatics as a building block via polymerization. The resulting polycarbolongs exhibit not only broad and strong UV−Vis absorptions but also good solubility. Many metallo-polymers have demonstrated a significant influence on the optical, electronic, and magnetic properties of the resulting materials (33, 41–48). Given that carbolong complexes have proved to be potent catalysts (49) and found wide applications in organic solar cells (26, 27), perovskite (50), photoacoustic imaging (51), and photo-thermal/photodynamic therapy (52, 53), it can be anticipated that polycarbolongs will show potential applications in catalysis, opto-electronics, and biotherapy. We will report these applications separately in subsequent articles.

Materials and Methods

Solvents were distilled from sodium/benzophenone (tetrahydrofuran, hexane, and diethyl ether) or calcium hydride (dichloromethane) under N_2 before use. Nondistilled solvents were used in the reactions carried out in air. The starting materials were used as received from commercial sources without further purification. Chromatography was performed on alumina gel (200–300 mesh) or silica gel (200–300 mesh) in air. All the calculations were performed with the Gaussian 09 software package. Details for all compounds and polymers reported here are given in the *SI Appendix*.

Author affiliations: ᵃState Key Laboratory of Physical Chemistry of Solid Surfaces, Collaborative Innovation Center of Chemistry for Energy Materials (iChEM), College of Chemistry and Chemical Engineering, Xiamen University, Xiamen 361005, China; and ᵇShenzhen Grubbs Institute and Department of Chemistry, Southern University of Science and Technology, Shenzhen 518005, China

1. A. J. Heeger, Semiconducting and metallic polymers: The fourth generation of polymeric materials (Nobel Lecture). *Angew. Chem. Int. Ed.* **40**, 2591–2611 (2001).
2. H. Shirakawa, The discovery of polyacetylene film: The dawning of an era of conducting polymers (Nobel Lecture). *Angew. Chem. Int. Ed.* **40**, 2574–2580 (2001).
3. A. G. MacDiarmid, "Synthetic metals": A novel role for organic polymers (Nobel Lecture). *Angew. Chem. Int. Ed.* **40**, 2581–2590 (2001).
4. J. R. Reynolds, B. C. Thompson, T. A. Skotheim, *Conjugated Polymers: Properties, Processing, and Applications* (CRC Press, ed. 4, 2019).
5. T. M. Swager, 50th anniversary perspective: Conducting/semiconducting conjugated polymers. a personal perspective on the past and the future. *Macromolecules* **50**, 4867–4886 (2017).
6. X. Guo, A. Facchetti, The journey of conducting polymers from discovery to application. *Nat. Mater.* **19**, 922–928 (2020).
7. L. R. MacFarlane et al., Functional nanoparticles through π-conjugated polymer self-assembly. *Nat. Rev. Mater.* **6**, 7–26 (2020).
8. S. Rochat, T. M. Swager, Conjugated amplifying polymers for optical sensing applications. *ACS Appl. Mater. Interfaces* **5**, 4488–4502 (2013).
9. C. Dai, B. Liu, Conjugated polymers for visible-light-driven photocatalysis. *Energy Environ. Sci.* **13**, 24–52 (2020).
10. A. J. Gillett et al., The role of charge recombination to triplet excitons in organic solar cells. *Nature* **597**, 666–671 (2021).
11. D. Meng et al., Near-infrared materials: The turning point of organic photovoltaics. *Adv. Mater.* **34**, 2107330 (2021).
12. Y. Li, Molecular design of photovoltaic materials for polymer solar cells: Toward suitable electronic energy levels and broad absorption. *Acc. Chem. Res.* **45**, 723–733 (2012).
13. M. S. Vezie et al., Exploring the origin of high optical absorption in conjugated polymers. *Nat. Mater.* **15**, 746–753 (2016).
14. H. Sun, X. Guo, A. Facchetti, A. High-performance n-type polymer semiconductors: Applications, recent development, and challenges. *Chem* **6**, 1310–1326 (2020).
15. S. Yum et al., Benzotriazole-containing planar conjugated polymers with noncovalent conformational locks for thermally stable and efficient polymer field-effect transistors. *Chem. Mater.* **26**, 2147–2154 (2014).
16. G. P. Kini, S. J. Jeon, D. K. Moon, Design principles and synergistic effects of chlorination on a conjugated backbone for efficient organic photovoltaics: A critical review. *Adv. Mater.* **32**, e1906175 (2020).
17. C. Sun et al., High efficiency polymer solar cells with efficient hole transfer at zero highest occupied molecular orbital offset between methylated polymer donor and brominated acceptor. *J. Am. Chem. Soc.* **142**, 1465–1474 (2020).
18. D. L. Thorn, R. Hoffmann, Delocalization in metallocycles. *Nouv. J. Chim.* **3**, 39–45 (1979).
19. D. Chen, Y. Hua, H. Xia, Metallaaromatic chemistry: History and development. *Chem. Rev.* **120**, 12994–13086 (2020).
20. B. J. Frogley, L. J. Wright, Recent advances in metallaaromatic chemistry. *Chemistry* **24**, 2025–2038 (2018).
21. L. J. Wright, *Metallabenzenes: An Expert View* (John Wiley & Sons Ltd, 2017).
22. Y. Zhang et al., Metalla-aromatics: Planar, nonplanar, and spiro. *Acc. Chem. Res.* **54**, 2323–2333 (2021).
23. C. Zhu et al., Stabilization of anti-aromatic and strained five-membered rings with a transition metal. *Nat. Chem.* **5**, 698–703 (2013).
24. Q. Zhuo et al., Multiyne chains chelating osmium via three metal-carbon σ bonds. *Nat. Commun.* **8**, 1912 (2017).
25. C. Zhu, H. Xia, Carbolong chemistry: A story of carbon chain ligands and transition metals. *Acc. Chem. Res.* **51**, 1691–1700 (2018).
26. S. Chen et al., Addition of alkynes and osmium carbynes towards functionalized dπ-pπ conjugated systems. *Nat. Commun.* **11**, 4651 (2020).
27. L. Liu et al., Nanographene-osmapentalyne complexes as cathode interlayer of organic solar cells enhanced efficiency over 18%. *Adv. Mater.* **33**, 2101279 (2021).
28. Y. Liu, J. W. Y. Lam, B. Z. Tang, Conjugated polymers developed from alkynes. *Natl. Sci. Rev.* **2**, 493–509 (2015).
29. T. Han et al., Facile multicomponent polymerizations toward unconventional luminescent polymers with readily openable small heterocycles. *J. Am. Chem. Soc.* **140**, 5588–5598 (2018).
30. H. Wang et al., Synthesis of self-healing polymers by scandium-catalyzed copolymerization of ethylene and anisylpropylenes. *J. Am. Chem. Soc.* **141**, 3249–3257 (2019).
31. O. M. Ogba, N. C. Warner, D. J. O'Leary, R. H. Grubbs, Recent advances in ruthenium-based olefin metathesis. *Chem. Soc. Rev.* **47**, 4510–4544 (2018).
32. H. Wang, X. Wu, Y. Yang, M. Nishiura, Z. Hou, Co-syndiospecific alternating copolymerization of functionalized propylenes and styrene by rare-earth catalysts. *Angew. Chem. Int. Ed. Engl.* **59**, 7173–7177 (2020).
33. C. L. Ho, Z. Q. Yu, W. Y. Wong, Multifunctional polymetallaynes: Properties, functions and applications. *Chem. Soc. Rev.* **45**, 5264–5295 (2016).

34. I. Manners, *Synthetic Metal-Containing Polymers* (John Wiley & Sons Ltd, 2002).
35. T. Shimura et al., Synthesis of poly(arylene cobaltacyclopentadienylene)s, a new class of organometallic π-conjugated polymers, by metallacycling polymerization and their physical properties. *Chem. Mater.* **8**, 1307–1315 (1996).
36. I. Matsuoka, K. Aramaki, H. Nishihara, Regioselective synthesis and electrochemical properties of π-conjugated cobaltacyclopentadiene oligomer and polymer complexes. *J. Chem. Soc., Dalton Trans.* **1**, 147–152 (1998).
37. M. R. Andersson, G. Yu, A. J. Heeger, Photoluminescence and electroluminescence of films from soluble PPV-polymers. *Synth. Met.* **85**, 1275–1276 (1997).
38. N. Tanigaki, H. Masuda, K. Kaeriyama, Substituted poly(p-phenylene)s prepared from 2,5-diheptylbenzene-1,4-bis(trimethylene boronate). *Polymer (Guildf.)* **38**, 1221–1226 (1997).
39. J. Gruber et al., Electrochemical synthesis, characterization and photophysics of a poly(fluorenylene vinylene) derivative. *Synth. Met.* **156**, 104–109 (2006).
40. C. Weder, M. S. Wrighton, Efficient solid-state photoluminescence in new poly(2,5-dialkoxy-p-phenyleneethynylene)s. *Macromolecules* **29**, 5157–5165 (1996).
41. R. A. Musgrave et al., Main-chain metallopolymers at the static–dynamic boundary based on nickelocene. *Nat. Chem.* **9**, 743–750 (2017).
42. Y. Yan, J. Zhang, L. Ren, C. Tang, Metal-containing and related polymers for biomedical applications. *Chem. Soc. Rev.* **45**, 5232–5263 (2016).
43. Y. Zhang et al., Distal conformational locks on ferrocene mechanophores guide reaction pathways for increased mechanochemical reactivity. *Nat. Chem.* **13**, 56–62 (2021).
44. L. Xu et al., Metallated graphynes as a new class of photofunctional 2D organometallic nanosheets. *Angew. Chem. Int. Ed. Engl.* **60**, 11326–11334 (2021).
45. F. Vidal, F. Jäkle, Functional polymeric materials based on main-group elements. *Angew. Chem. Int. Ed. Engl.* **58**, 5846–5870 (2019).
46. G. R. Whittell, M. D. Hager, U. S. Schubert, I. Manners, Functional soft materials from metallopolymers and metallosupramolecular polymers. *Nat. Mater.* **10**, 176–188 (2011).
47. Q. Dong et al., A molecular approach to magnetic metallic nanostructures from metallopolymer precursors. *Chem. Soc. Rev.* **47**, 4934–4953 (2018).
48. Y. Cha et al., Mechanochemistry of cationic cobaltocenium mechanophore. *J. Am. Chem. Soc.* **143**, 11871–11878 (2021).
49. F.-H. Cui et al., Selective difunctionalization of unactivated aliphatic alkenes enabled by a metal–metallaaromatic catalytic system. *J. Am. Chem. Soc.* **144**, 2301–2310 (2022).
50. J. Wang et al., Tuning an electrode work function using organometallic complexes in inverted perovskite solar cells. *J. Am. Chem. Soc.* **143**, 7759–7768 (2021).
51. C. Zhu et al., Stabilizing two classical antiaromatic frameworks: Demonstration of photoacoustic imaging and the photothermal effect in metalla-aromatics. *Angew. Chem. Int. Ed. Engl.* **54**, 6181–6185 (2015).
52. C. Zhu et al., CCCCC pentadentate chelates with planar Möbius aromaticity and unique properties. *Sci. Adv.* **2**, e1601031 (2016).
53. N. Lu et al., An osmium-peroxo complex for photoactive therapy of hypoxic tumors. *Nat. Commun.* **13**, 2245 (2022).
54. S. Chen et al., Conjugated polymers based on metalla-aromatic building blocks. CCDC : 2057490 (1b). https://www.ccdc.cam.ac.uk/structures/Search?Ccdcid=2057490&DatabaseToSearch=Published. Deposited 20 January 2021.
55. S. Chen et al., Conjugated polymers based on metalla-aromatic building blocks. CCDC : 2057491 (2b). https://www.ccdc.cam.ac.uk/structures/Search?Ccdcid=2057491&DatabaseToSearch=Published. Deposited 20 January 2021.
56. S. Chen et al., Conjugated polymers based on metalla-aromatic building blocks. CCDC : 2057492 (3). https://www.ccdc.cam.ac.uk/structures/Search?Ccdcid=2057492&DatabaseToSearch=Published. Deposited 20 January 2021.
57. S. Chen et al., Conjugated polymers based on metalla-aromatic building blocks. CCDC : 2142032 (8). https://www.ccdc.cam.ac.uk/structures/Search?Ccdcid=2142032&DatabaseToSearch=Published. Deposited 14 January 2021.
58. S. Chen et al., Conjugated polymers based on metalla-aromatic building blocks. CCDC : 2057497 (L3). https://www.ccdc.cam.ac.uk/structures/Search?Ccdcid=2057497&DatabaseToSearch=Published. Deposited 20 January 2021.